1	PROTOLITH AFFILIATION AND TECTONOMETAMORPHIC EVOLUTION OF THE
2	GURLA MANDHATA CORE COMPLEX, NW NEPAL HIMALAYA
3	LAURENT GODIN <sup>1†</sup> , MARK AHENDA <sup>1</sup> , DJORDJE GRUJIC <sup>2</sup> , ROSS STEVENSON <sup>3</sup> , AND JOHN COTTLE <sup>4</sup>
4 5	<sup>1</sup> Geological Sciences and Geological Engineering, Queen's University, Kingston, Ontario, Canada, K7L 3N6
6 7	<sup>2</sup> Department of Earth and Environmental Sciences, Dalhousie University, 1459 Oxford Street, Halifax, NS B3H 4R2, Canada
8 9 10 11	<ul> <li><sup>3</sup> GÉOTOP and Département des Sciences de la Terre et de l'Atmosphère - Université du Québec à Montréal, C.P. 8888, Succursale Centre-Ville, Montréal, QC, Canada H3C 3P8</li> <li><sup>4</sup> Department of Earth Science, University of California, Santa Barbara, CA 93106-9630, USA</li> </ul>
12	SUPPLEMENTARY FILE 1
13	
14	
15	1A. Sm-Nd analytical procedures
16	1B. U-Th/Pb petrochronology and analytical procedures
17	1C. Supplementary back-scattered electron imagery and X-ray ion microprobe chemical
18	maps
19	1D. References
20	

22

## 1A. Sm-Nd analytical procedures

Rock samples were crushed and pulverized using a ceramic mortar and pestle, then
dissolved using lithium borate fusion and analyzed on ICP-ES for major elements and ICP-MS
for Rare Earth Elements (REEs) and other trace elements.

26 Sm-Nd isotopic analyses were performed at GÉOTOP – Université du Québec à

27 Montréal. 80-110 mg of powder of each sample was spiked with a <sup>150</sup>Nd/<sup>149</sup>Sm-enriched spike

and dissolved in a mixture of 15N HNO3 and 29N HF over 5-7 days. The resulting fluoride salts

29 were treated with 16N HNO3 and 6N HCl to dissolve and enhance the solubility of the REEs.

30 Iron was removed by loading samples in ion-exchange polyprep columns with AG1X8 resin and

31 6N HCl. The REEs were isolated with TRU Spec resin using 0.05N HNO3, and Nd and Sm were

32 separated with LN Spec resin using 0.2N, 0.3N, and 0.5N HCl. The Nd and Sm fractions were

33 loaded onto Re filaments and analyzed on a TRITON PLUS thermal ionization mass

34 spectrometer (TIMS) in static mode. Mass fractionation was corrected using the ratio

 $^{146}$ Nd/ $^{144}$ Nd = 0.7129 assuming exponential fractionation behavior. The Nd isotopic

36 compositions are expressed as  $\varepsilon Nd_{(0)}$  and calculated using the present day chondritic uniform

37 reservoir (CHUR) values of  ${}^{143}$ Nd/ ${}^{144}$ Nd = 0.512639 and  ${}^{147}$ Sm/ ${}^{144}$ Nd = 0.1966 (Goldstein et al.,

38 1984). The <sup>147</sup>Sm/<sup>144</sup>Nd ratios are accurate to 0.5%, corresponding to an average  $\epsilon$ Nd(0) error of

 $\pm 0.5$  epsilon units, based on measurements of the JNdi Nd standard ( $^{143}$ Nd/ $^{144}$ Nd = 0.512095 $\pm 5$ ,

40 n=3).

41

42 1B. U-Th/Pb petrochronology and analytical procedures

43 Petrochronology is the interpretation of isotopic dates in light of complementary
44 elemental or isotopic information from the same mineral(s) (Kylander-Clark et al., 2013).
45 Yttrium (Y) zonation is a key component of monazite petrochronological interpretation. Y is

46 readily incorporated in the crystal lattice of monazite (Pyle et al., 2001). In metapelitic rocks, 47 however, garnet preferentially incorporates Y and heavy rare earth elements (HREEs) during 48 growth, depleting the free Y and HREE content of the system and leaving monazites that grew in 49 the presence of garnet Y-poor (Spear and Pyle, 2002; Pyle and Spear, 2003; Kohn et al., 2005). 50 Garnet breakdown during anatexis or decompression can release Y into the system, causing any 51 concurrently crystallizing monazite to be higher in Y content (Pyle, et al., 2001). Monazite 52 results in garnet-bearing rocks can be linked to stages of garnet growth and breakdown, and 53 therefore to prograde or retrograde metamorphism. In melt-present systems, monazite can 54 dissolve on the prograde path during partial melting but tends to recrystallize on the retrograde 55 path, still resulting in higher Y and HREE content in retrograde monazites (Kelsey et al., 2008). 56 Monazite grains were identified in thin section and selected using a Mineral Liberation 57 Analysis 650 field emission gun environmental scanning electron microscope at Queen's Facility 58 for Isotope Research (Queen's University, Kingston, Ontario, Canada). Selected grains were 59 chemically mapped for U, Th, Y, Ca, and Si with X-ray wavelength dispersive spectrometry on a 60 JEOL JXA-8230 electron microprobe, also at Queen's Facility for Isotope Research. The 61 electron microprobe experimental conditions were set at an acceleration voltage of 15 kV, beam 62 current of 200 nA, dwell time of 100 ms and step size of 0.5-1.4 µm. X-ray element maps 63 identified chemical zonation and informed laser spot locations. 64 Monazite was analyzed directly in thin section using the Laser Ablation Split Stream 65 (LASS) method at the University of California Santa Barbara. Spot location was guided with the 66 aid of X-ray compositional maps. Instrumentation consists of a Photon Machines 193 nm ArF 67 Excimer laser and 'HelEx' ablation cell coupled to a Nu Instruments HR Plasma high-resolution

68 multi-collector MC-ICP-MS (U, Th, and Pb isotopes) and an Agilent 7700S Quadrupole ICP-MS

69 (major and trace elements). Methods in this study follow those outlined in Kylander-Clark et al. 70 (2013) with modifications outlined in McKinney et al. (2015). Monazite was ablated using a 7 71  $\mu$ m diameter spot at 3 Hz repetition rate for 90 shots at a laser fluence of 1.5 J/cm2, resulting in 72 craters that are ~4  $\mu$ m deep.

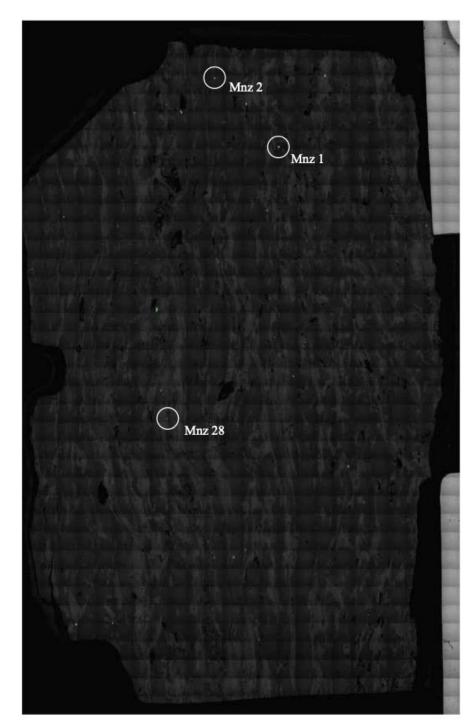
Data reduction, including corrections for baseline, instrumental drift, mass bias, down-73 74 hole fractionation as well as age calculations were carried out using Iolite v. 2.5 (Paton et al. 75 2010). Background intensities and changes in instrumental bias were interpolated using a 76 smoothed cubic spline while down-hole inter-element fractionation was modeled using an 77 exponential function. Statistics for baselines, on peak intensities and isotopic ratios were calculated using the mean with a 2.S.D. outlier rejection. The <sup>238</sup>U and <sup>235</sup>U decay constants of 78 Jaffey et al. (1971) and the <sup>232</sup>Th decay constant of Amelin and Zaitsev (2002) were employed to 79 80 calculate ages. All uncertainties are quoted at  $2\sigma$  and include contributions from the external reproducibility of the primary reference material for the <sup>206</sup>Pb/<sup>238</sup>U ratios and <sup>208</sup>Pb/<sup>232</sup>Th ratios. 81 Monazite U-Th/Pb data was normalized to '44069' (424 Ma<sup>207</sup>Pb/<sup>235</sup>U ID-TIMS age, 82 Aleinikoff et al. 2006), employed to monitor and correct for mass bias as well as Pb/U and Pb/Th 83 84 down-hole fractionation. To monitor data accuracy, a reference monazite 'FC-1' (55.7 Ma 85 <sup>206</sup>Pb/<sup>238</sup>U ID-TIMS age, Horstwood et al. 2003) was analyzed concurrently (once every ~7 86 unknowns) and mass bias- and fractionation-corrected based on measured isotopic ratios of the 87 primary reference material. During the analytical period, 21 analyses of FC-1 gave a weighted 88 mean  ${}^{206}\text{Pb}/{}^{238}\text{U}$  date of 56.0 ± 1.0 Ma, and a weighted mean  ${}^{208}\text{Pb}/{}^{232}\text{Th}$  date of 55.2 ± 0.9 Ma. 89 Trace element data were normalized to 'Bananeira' monazite using P as an internal 90 standard and the concentration values reported in Kylander-Clark et al., (2013). Si, Ca, and Mg 91 levels were monitored for evidence of inclusions and ablation sites visually inspected to ensure

- 92 no contamination occurred during analysis. Based on the long-term reproducibility of multiple
- 93 secondary reference minerals, trace element concentrations are accurate to better than 5% ( $2\sigma$ ).

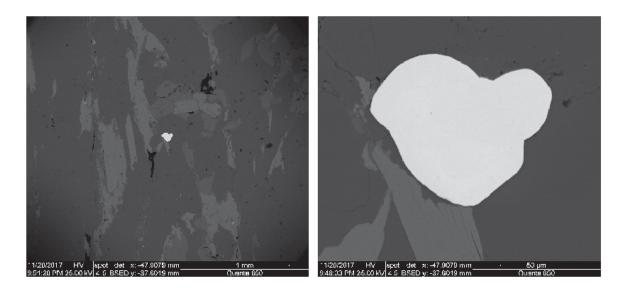
94

- 96 1C. Supplementary back-scattered electron imagery and X-ray ion microprobe chemical
- 97 maps





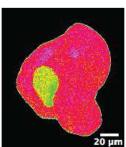
## MA-06 mnz 1



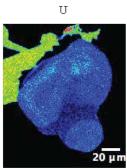
Y







Са



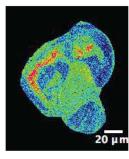
SL

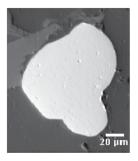
BSE

20 µm

Th

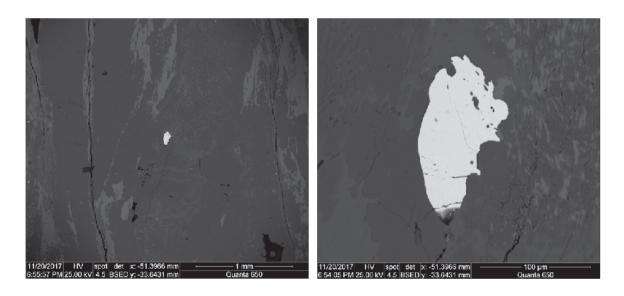








## MA-06 mnz 2

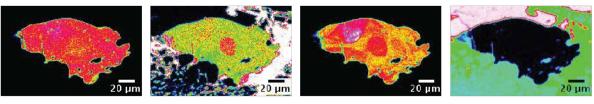


Y

U

Th

Si

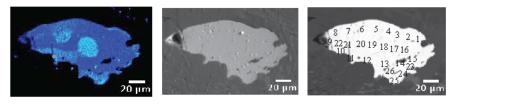


Са

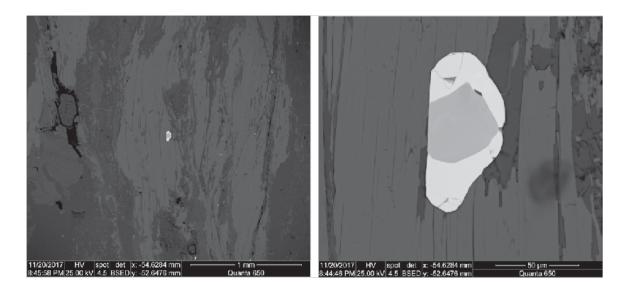


SL

BSE



## MA-06 mnz 28

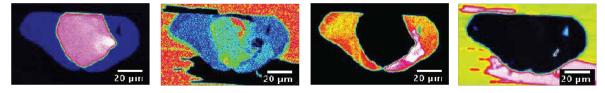


Y

U

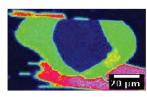
Th

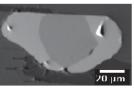
Si



Са

BSE

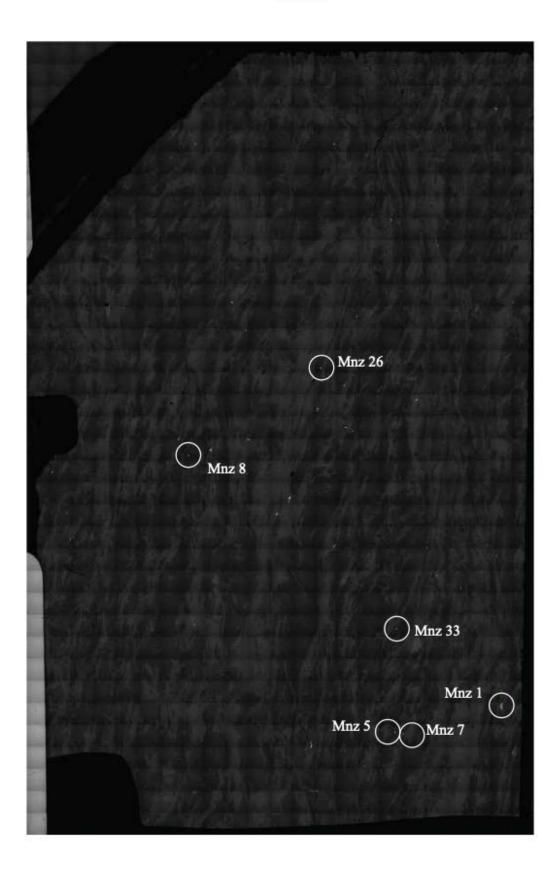


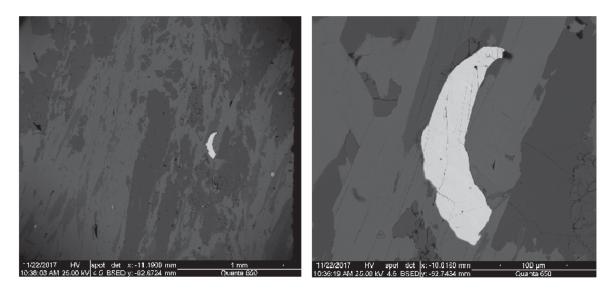


SL

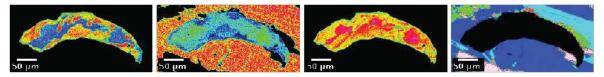








Si



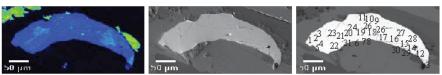
Са

Y

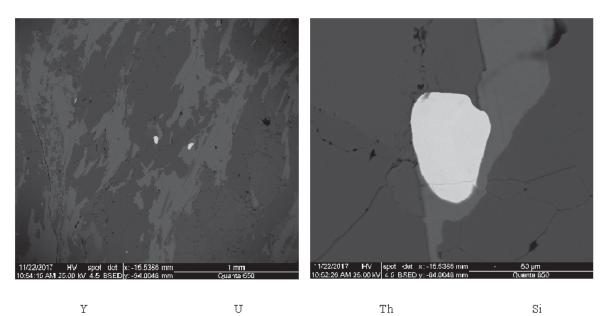
SL

BSE

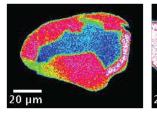
Th

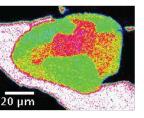


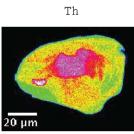
U

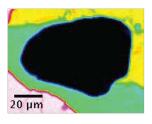


U





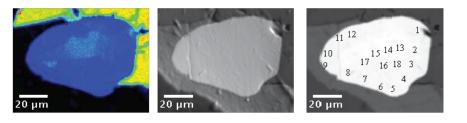


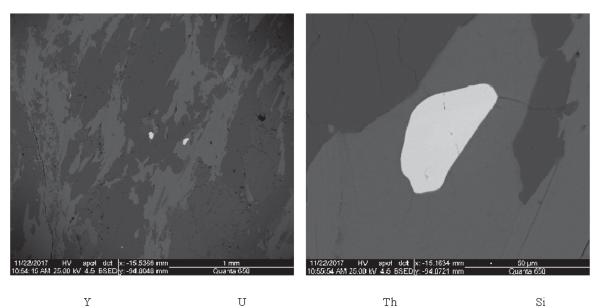


Са

SL

BSE

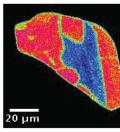


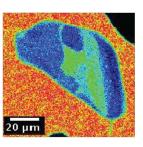


Y

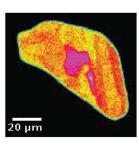
U

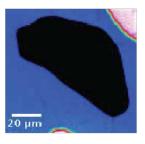






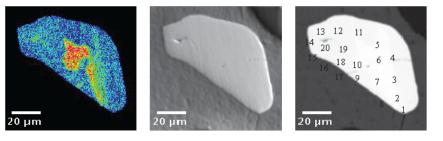
 $\operatorname{SL}$ 

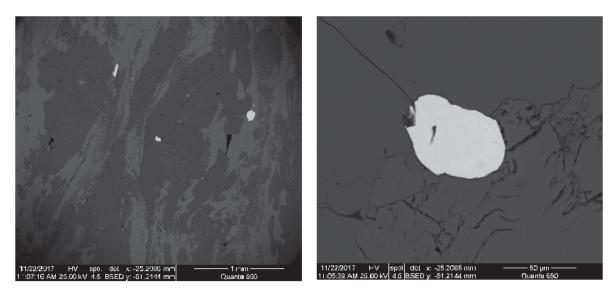


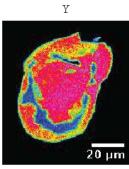


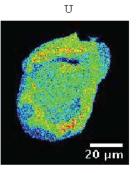
Са

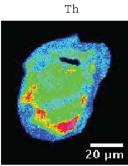
BSE

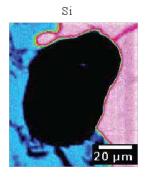




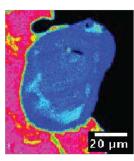


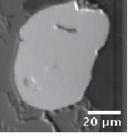




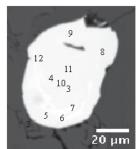


Са



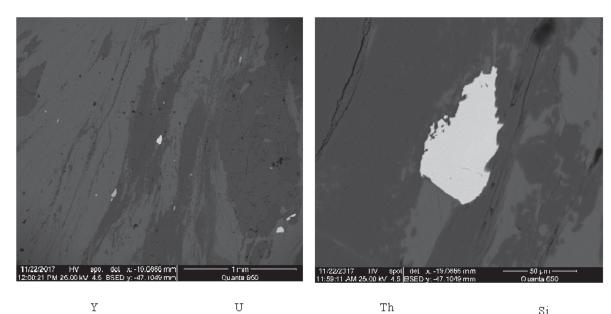


SL



BSE



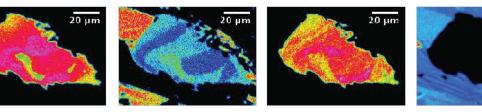


Υ

Th

Si

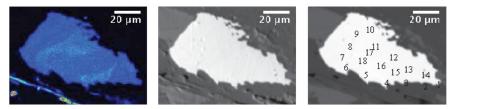
20 µm

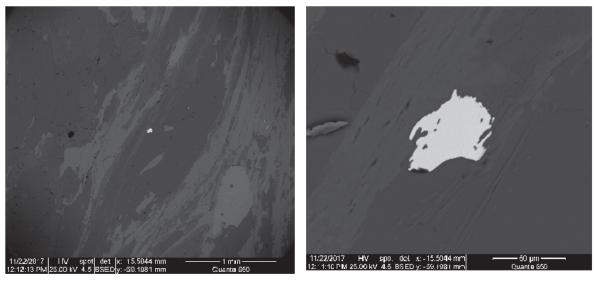


Са



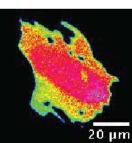
BSE

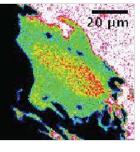




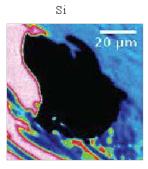
Y

U

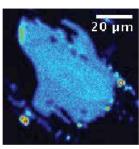


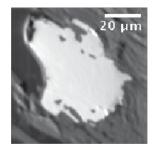


Τh 20 µm

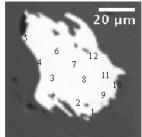


Са



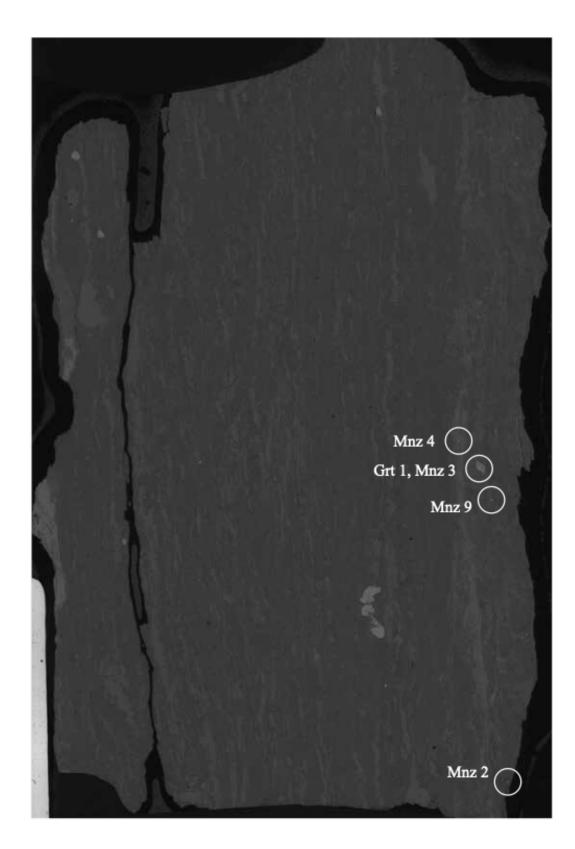


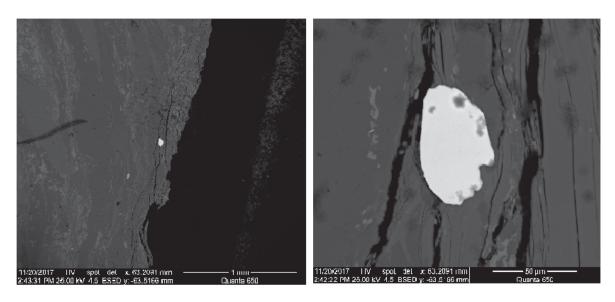
SL

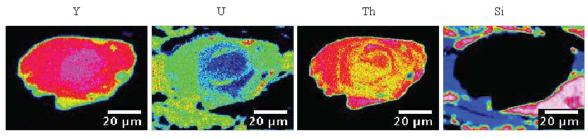


BSE





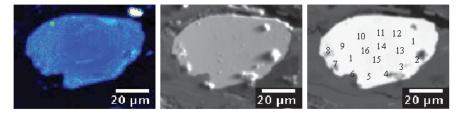


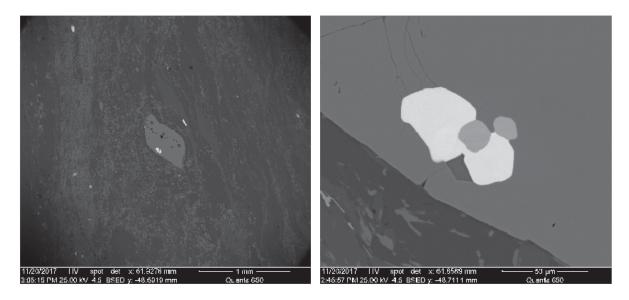


Са

SL

BSE

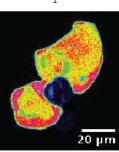




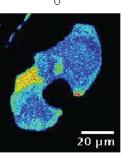
Y

U

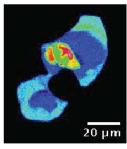
Si



Са



SL

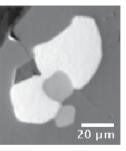


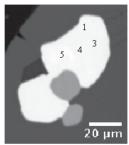
Th

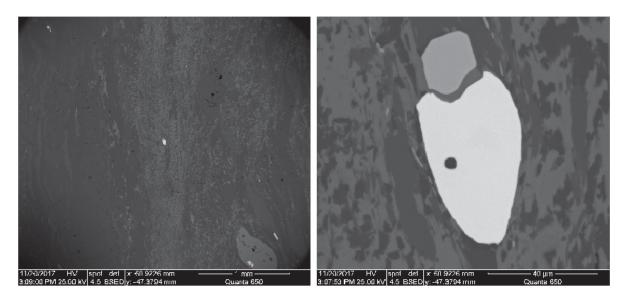
BSE

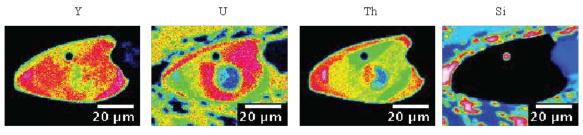


<u>20 µm</u>



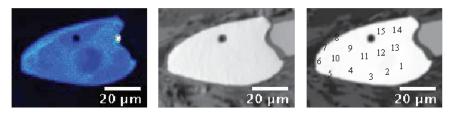




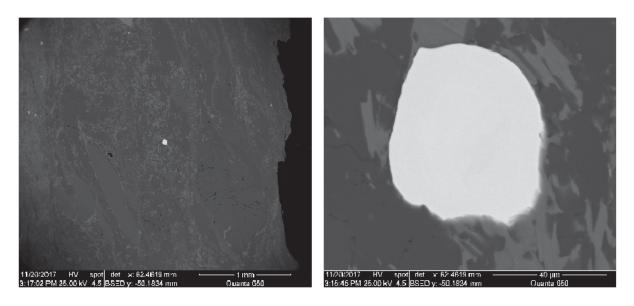


Са

BSE

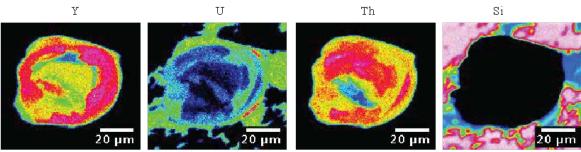


SL

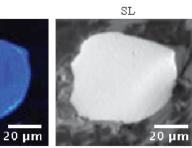


Y

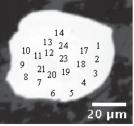
U



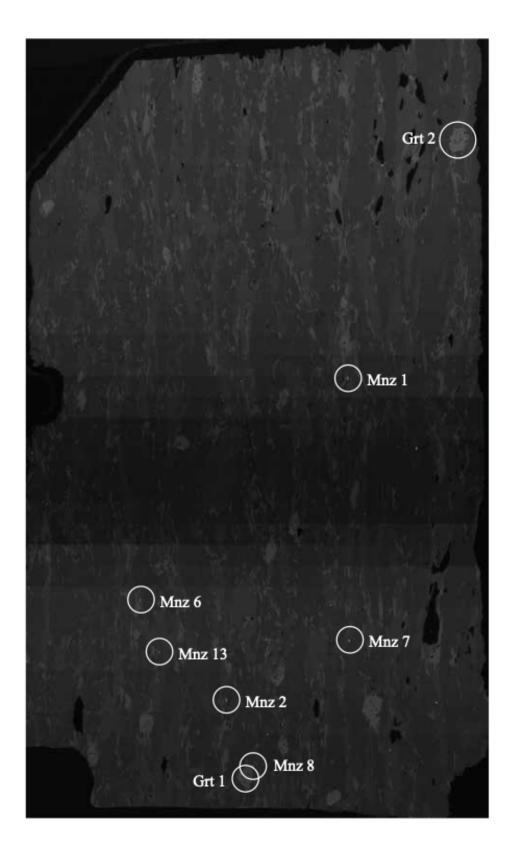
Са

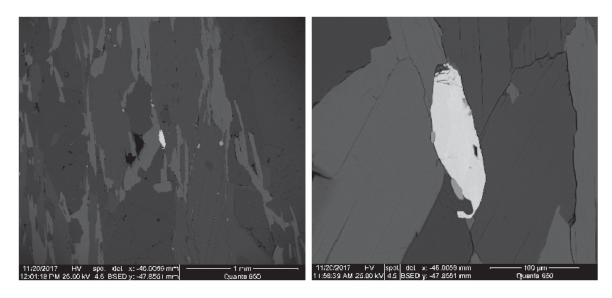










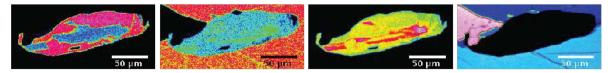


Y

U

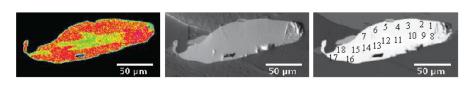
Th

Si

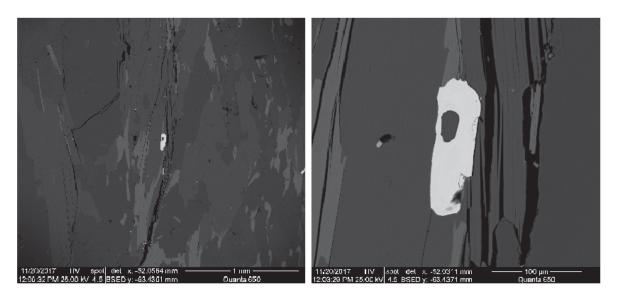


Са

BSE

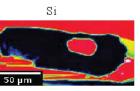


SL



U

50



Са

50

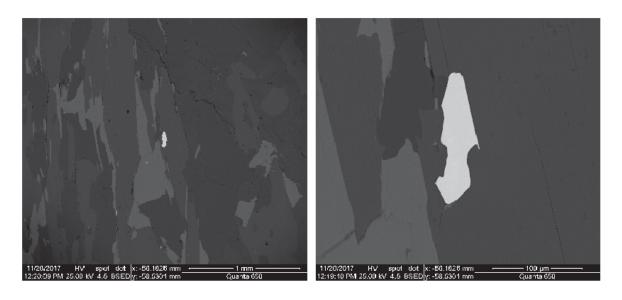
Y

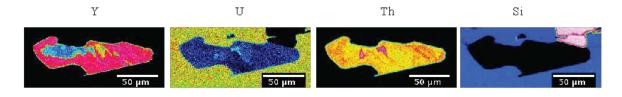
SL

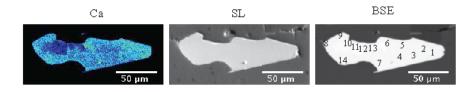
BSE

Τh

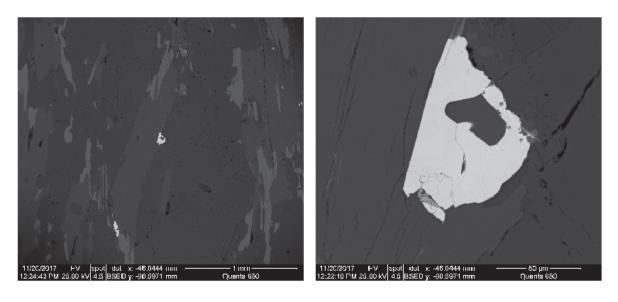








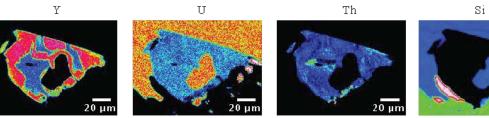
MA-26 mnz 7



Y

U

20 µm

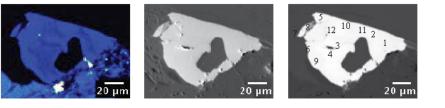


Са

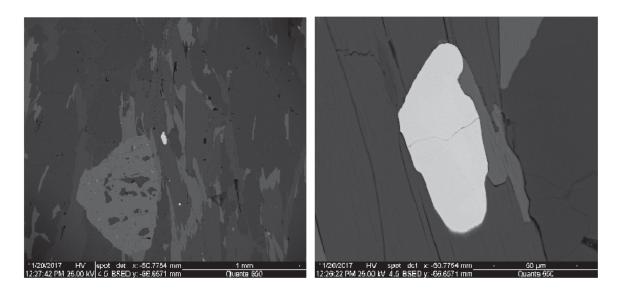




BSE



 $\operatorname{SL}$ 

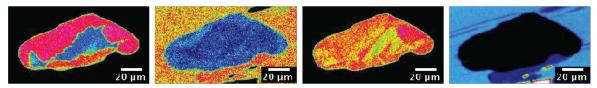


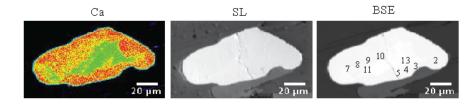
Y

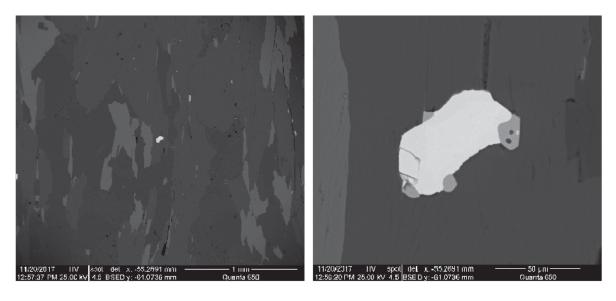
U

Th

Si

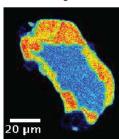


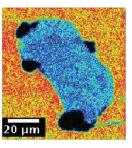


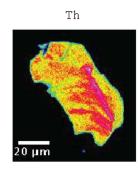


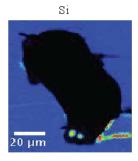
Y

U





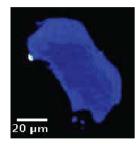


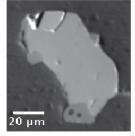


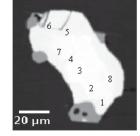
Са

SL

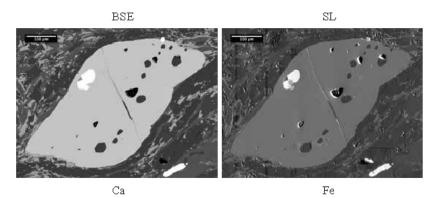
BSE

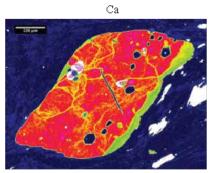






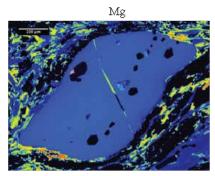


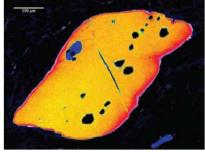


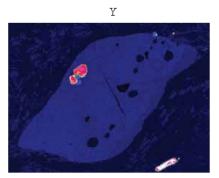




Mn

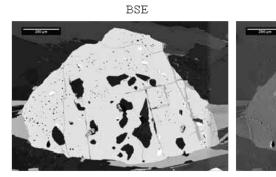




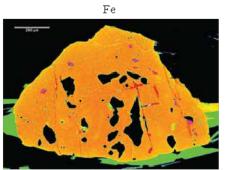




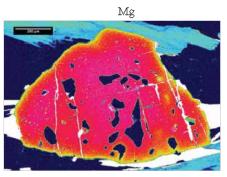
SL

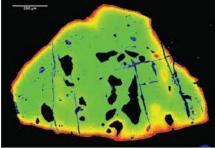


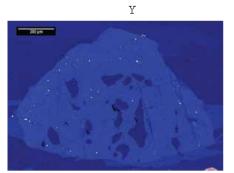
Са



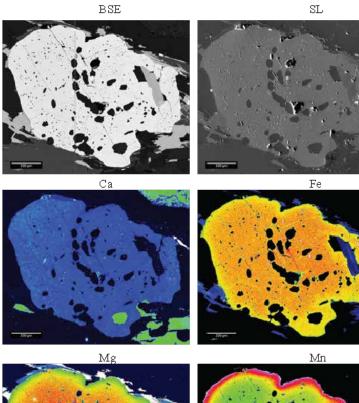
Mn

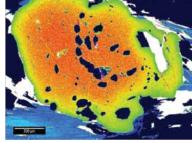


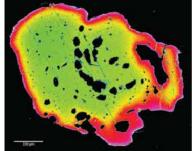


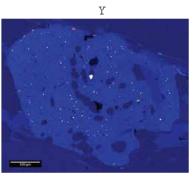












- **2C. U-Th/Pb monazite petrochronology data available in a separate Excel file**

# 172 **1D. References**

173 Aleinikoff, J.N., Schenck, W.S., Plank, M.O., Srogi, L., Fanning, C.M., Kamo, S.L., and 174 Bosbyshell, H., 2006, Deciphering igneous and metamorphic events in high-grade rocks 175 of the Wilmington Complex, Delaware: Morphology, cathodoluminescence and 176 backscattered electron zoning, and SHRIMP U-Pb geochronology of zircon and 177 monazite: Geological Society of America Bulletin, v. 118(1-2), p. 39-64. 178 Amelin, Y. and Zaitsev, A.N., 2002' Precise geochronology of phosphorites and carbonatites: 179 The critical role of U-series disequilibrium in age interpretations: Geochimica 180 Cosmochimica Acta, v. 66, p. 2399–2419. 181 Goldstein, S., Onions, R., and Hamilton, P., 1984, A Sm-Nd isotopic study of atmospheric 182 dustsand particulates from major river systems: Earth and Planetary Science Letters, v. 183 70, p. 221–236, doi: 10.1016/0012-821x(84)90007-4. 184 Horstwood, M.S.A., Foster, G.L., Parrish, R.R., Noble, S.R., Nowell, G.M., 2003, Common-Pb 185 corrected in situ U-Pb accessory mineral geochronology by LA-MC-ICP-MS: Journal of 186 Analytical Atomic Spectrometry, v. 18, p. 837–846, doi.org/10.1039/b304365g. 187 Jaffey, A.H., Flynn, K.F., Glendenin, L.E., Bentley, W.C., Essling, A.M., 1971, Precision 188 measurement of the half-lives and specific activities of U235 and U238: Physical 189 Reviews, C4, p. 1889–1906, doi.org/10.1103/PhysRevC.4.1889. 190 Kelsey, D.E., Clark, C., and Hand, M., 2008, Thermobarometric modelling of zircon and 191 monazite growth in melt-bearing systems: examples using model metapelitic and 192 metapsammitic granulites: Journal of Metamorphic Geology, v. 26, p. 199-212, doi: 193 10.1111/j.1525-1314.2007.00757.x. 194 Kohn, M.J., Wieland, M.S., Parkinson, C.D., and Upreti, B.N., 2005, Five generations of monazite in Langtang gneisses: implications for chronology of the Himalayan 195 196 metamorphic core: Journal of Metamorphic Geology, v. 23, p. 399–406, doi: 197 10.1111/j.1525-1314.2005.00584.x. 198 Kylander-Clark, A.R., Hacker, B.R., and Cottle, J.M., 2013, Laser-ablation split-stream ICP 199 petrochronology: Chemical Geology, v. 345, p. 99-112, doi: 200 10.1016/j.chemgeo.2013.02.019. 201 McKinney, S.T., Cottle, J.M., and Lederer, G.W., 2015, Evaluating rare earth element (REE) 202 mineralization mechanisms in Proterozoic gneiss, Music Valley, California: Geological 203 Society of America Bulletin, doi: 10.1130/b31165.1. 204 Paton, C., Woodhead, J.D., Hellstrom, J.C., Hergt, J.M., Greig, A., and Maas, R., 2010, 205 Improved laser ablation U-Pb zircon geochronology through robust downhole 206 fractionation correction: Geochemistry, Geophysics, Geosystems, v. 11, doi: 207 10.1029/2009gc002618.

Pyle, J.M., Spear, F.S., Rudnick, R.L, and McDonough, W.F., 2001, Monazite-Xenotime-Garnet
 Equilibrium in Metapelites and a New Monazite-Garnet Thermometer: Journal of
 Petrology, v. 42, p. 2083–2107, doi: 10.1093/petrology/42.11.2083.

# Pyle, J.M., and Spear, F.S., 2003, Four generations of accessory-phase growth in low-pressure migmatites from SW New Hampshire: American Mineralogist, v. 88, p. 338–351, doi: 10.2138/am-2003-2-311.

Spear, F.S., and Pyle, J.M., 2002, Apatite, Monazite, and Xenotime in Metamorphic Rocks:
Reviews in Mineralogy and Geochemistry, v. 48, p. 293–335, doi:
10.2138/rmg.2002.48.7.

217

218